Polymer 51 (2010) 2221–2228

Contents lists available at ScienceDirect

Polymer

journal homepage: www.elsevier.com/locate/polymer

Wall slip and melt-fracture of polystyrene melts in capillary flow

Ryohei Komuro [a], Koji Kobayashi [a], Takashi Taniguchi [b], Masataka Sugimoto [a], Kiyohito Koyama [a,*]

[a] Graduate School of Science and Engineering, Yamagata University, Yonezawa, Yamagata 992-8510, Japan
[b] Department of Chemical Engineering, Kyoto University, Kyoto 615-8510, Japan

ARTICLE INFO

Article history:
Received 1 October 2009
Received in revised form
16 February 2010
Accepted 4 March 2010
Available online 15 March 2010

Keywords:
Slip velocity
Melt-fracture
Polystyrene

ABSTRACT

We investigated slip and unstable flow phenomena of polystyrene melts in capillaries from the view of the effects of temperature and molecular weight by using three polystyrene samples with different molecular weights ($M_w = 192{,}000$, $M_w = 258{,}000$, and $M_w = 321{,}000$). The slip velocities are estimated by the Mooney method and the modified Mooney method. We found that the slip velocity increases and the critical slip stress $\sigma_c^{(s)}$ above which a slip starts to occur decreases with the temperature. We also observed the melt-fracture at above a critical melt-fracture stress $\sigma_c^{(m)}$ higher than $\sigma_c^{(s)}$. We found that the onset of melt fracture is affected by the extensional stress near the entry region to the capillary in the barrel and the melt-fracture tends to easily occur with increase of the molecular weight, but is not sensitive to the temperature.

1. Introduction

In industrial processes such as extrusion and injection molding, molten plastics experiences a flow with a high shear rate especially near a wall of die. In such situations, molten polymeric materials exhibit unstable flow behaviors such as sharkskin and melt-fractures at above a certain critical shear stress at the wall of die. It has been recognized that the sharkskin behaviors are highly related to a slip phenomenon that takes place near the wall. Generally, the slip phenomenon of molten polymers at the wall has been investigated by the Mooney method [1] using the capillary rheometer. Kalita et al. [2] have concluded that the slippage at the wall of die is the origin of sharkskin phenomenon from their experimental evidences. Ramamurthy [3] has investigated the effect of wall material on the onsets of slippage and melt-fracture using linear low density polyethylene (LLDPE), high density polyethylene (HDPE) and a low density branched polyethylene (LDPE). He found that the critical stress for slippage depends on the material of die. It has been reported by Hatzikiriakos et al. [9] that in HDPE a slippage occurs at above a critical shear stress $\sigma_c^{(s)}$, and the slip velocity V_S obtained by the Mooney and the modified Mooney method satisfies the following empirical formula:

$$V_S = a \cdot (\sigma_w)^m. \quad (1)$$

They have also reported that the exponent m is not a function of temperature, but the coefficient a increases with temperature. For the onset of melt-fracture, it is now generally accepted that the melt-fracture is initiated at the entrance to the die from the barrel where the melt undergoes mainly a uniaxial extension due to the contraction flow. Moreover, it has been recognized that the melt-fracture occurs above a certain critical shear stress where a spiraling flow at the entrance of die becomes prominent [4–7]. Ballenger et al. [4,5] have investigated flow patterns of three polymer melts (LDPE, polystyrene (PS) and polypropylene (PP)) at the entrance region of capillary (entry angle $2\alpha = 180°$, see Fig. 1 for the definition of the entry angle) over a wide range of flow rates. They have reported that a spiraling motion at the entrance of die occurs at above a certain critical shear rate $\dot{\gamma}_C^{(m)}$ ($44\ s^{-1} \le \dot{\gamma}_C^{(m)} \le 96\ s^{-1}$), and then a distorted extrudate with a helical form appears. From a large number of studies on the melt-fracture phenomena [4–8], it is found that the melt-fracture is greatly affected by the extensional flow at the inlet of capillary.

Generally, the unstable flow behaviors in capillary can be classified into two types, I and II. In the type I unstable flow, with increasing a shear stress, a sharkskin of the surface of extrudate is observed firstly at above a first critical wall shear stress and then a melt-fracture is observed at above a second critical wall shear stress much larger than the first one. In the type II, on the other hand, with increasing a shear stress, an unstable flow with a helical-shaped extrudate occurs at above a first critical wall shear stress, and then the unstable flow become a melt-fracture at a second critical wall shear stress much larger than the first one. Actually, the reports on the slippage in materials which exhibit the type II

* Corresponding author. Tel.: +81 238 26 3055; fax: +81 238 26 3411.
E-mail address: koyama@yz.yamagata-u.ac.jp (K. Koyama).

0032-3861/$ – see front matter © 2010 Elsevier Ltd. All rights reserved.
doi:10.1016/j.polymer.2010.03.014

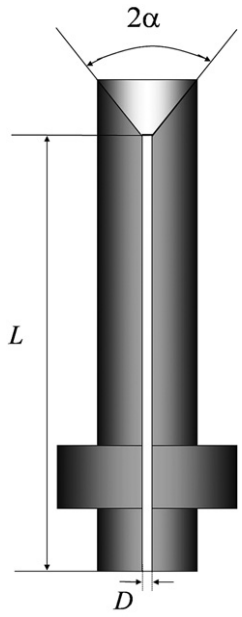

Fig. 1. Schematic diagram of die used in the present work.

unstable flow (hereafter we will refer such materials to type II materials) are not so many, therefore the slip phenomenon in type II materials is not well-understood. The type I unstable flow is observed in LLDPE, HDPE and LDPE samples, on the other hand, the type II is observed in PS and PP samples. These unstable flows have been widely reviewed by researchers about the past half-century. In most studies on unstable flow behaviors after 70's, resins that show the type I unstable flow have been used, since in such materials a shark skin can be occurred easily and the mechanism of sharkskin phenomenon has not been well-understood. Understanding of the sharkskin phenomenon is the key to control the process and to make the quality of product better at lower costs. The kind of sample used in such investigations of slippage concentrates on those of type I. On the other hand, the unstable flow phenomena and slippage in type II samples have not been well-understood since these samples have not been paid attention so much.

Therefore, the aim of the present work is to investigate slip phenomena and unstable flow phenomena in PS melts as one of type II samples, by using a capillary rheometer. Furthermore, we explore the effect of wall material on the slip phenomena of PS melts.

2. Experimental

2.1. Materials

We used three types of PS (PS1-3) that have different molecular weights. These samples are kindly supplied from Japan Polystyrene Inc. The weight-average molecular weights M_w and the polydispersity M_w/M_n for these samples are shown in Table 1, M_n being the number-average molecular weights. Since commercial samples usually contain mineral oils and it is considered that such mineral oils play important role in slip phenomenon *i.e.*, work as lubricants, we used PS samples that do not contain any mineral oils to remove the effect of the oil.

2.2. Rheological techniques

The temperature dependences of the linear viscoelasticity of PS1-3 are measured by linear dynamic shear experiments. The measurements are carried out with a rotational rheometer (Anton Paar GmbH, Austria, Physica, MCR301). The geometry of jig we used is parallel plate with the diameter 25 mm. The gap width is set to 1 mm. Circular disks of PS samples are prepared by compression moldings at 180 °C. All the experiments are performed at the following five temperatures 180, 195, 210, 225, and 240 °C under a nitrogen atmosphere. However, we could not make measurements at a temperature greater than or equal to 250 °C since the samples were degraded during the measurements.

Table 1
Polymeric samples used in the present work.

Sample	M_w	M_w/M_n
PS1	192,000	2.4
PS2	258,000	2.2
PS3	321,000	2.6

Using a capillary rheometer we measured the applied pressure P and volumetric flow rate Q. In order to reduce the effect of pressure loss at the entrance region to the capillary from the barrel, we used dies with an entry angle ($2\alpha = 60°$) and with an enough length L (see Fig. 1 and Table 2). In order to investigate the effect of die materials on the slip phenomenon, we used dies made of three kinds of materials with an entry angle ($2\alpha = 180°$) as shown in Table 2. In addition, we investigated on the slippage and unstable flow of PS1-3 by using the S25C dies to clarify the effect of molecular weight and temperature on the behavior of capillary flow of PS. All the experiments were performed at temperatures 180, 210, and 240 °C to elucidate the temperature dependence of capillary flow behavior of PS.

2.3. Capillary rheometry

The raw data in capillary rheometers are the applied pressure P and the piston speed. The volumetric flow rate Q can be calculated by the cross section of barrel and the piston speed. The shear stress σ_w at the wall and apparent shear rate $\dot{\gamma}_A$ are calculated from following equations:

$$\sigma_w = \frac{D}{4L}\Delta P \tag{2}$$

$$\dot{\gamma}_A = \frac{32Q}{\pi D^3} \tag{3}$$

The pressure difference ΔP between the pressures at the entry and the exit of die can be estimated through the Bagley correction where the applied pressure P are plotted as functions of the ratio of the length of capillary L to the diameter D, i.e., L/D by using at least three types of capillaries die and at various piston speeds. The equation for the shear rate Eq. (3) is valid only for the Newtonian fluid in the absence of wall slip. If there is no slip at the wall of capillary, the apparent shear flow $\dot{\gamma}_A$ for non-Newtonian fluid can be corrected to be $\dot{\gamma}_w$ by the Rabinowitsch correction as

Table 2
Capillary dies used in the present work and their kinds of materials. L and D denote the length and diameter of the capillary, respectively.

Diameter (D) [cm]	L/D	Entry Angle 2α	Material of Die
0.10	5, 10, 20	180°	S25C, Al, HCr
0.10	50	60°	S25C
0.15	33	60°	S25C
0.20	25	60°	S25C

S25C: Iron containing 0.22–0.28 wt% carbon.
Al: Aluminum.
HCr: Chrome-plated S25C.

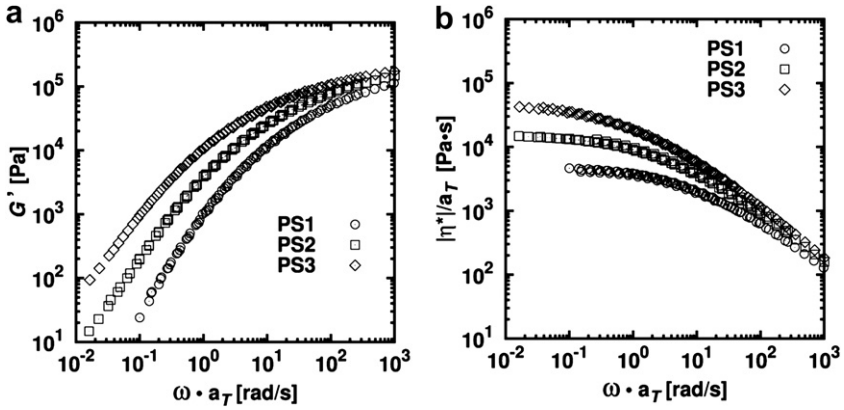

Fig. 2. Master curves of (a) the storage modulus G' and (b) the magnitude of complex viscosity $|\eta^*|$ of PS1-3 as a function of frequency of oscillatory shear. The reference temperature T_r to the master curves is set to 210 °C. The data at the five temperatures 180, 195, 210, 225 and 240 °C are superposed using the shift factor a_T.

$$\dot{\gamma}_w = \frac{1}{4}\dot{\gamma}_A\left(3 + \frac{d\ln\dot{\gamma}_A}{d\ln\sigma_w}\right). \tag{4}$$

If a slippage takes place at the wall, however, the Rabinowitsch correction cannot be applied to obtain the corrected shear rate for non-Newtonian fluid. Therefore, we used apparent shear rate $\dot{\gamma}_A$ to analyze whether a slip takes place or not, and to estimate the slip velocity. If a slippage takes place at the wall, the slip velocity V_S at the wall is estimated by the following equation as

$$\dot{\gamma}_A = \frac{8V_S(T)}{D} + \frac{4}{3\sigma_w^3}\int_0^{\sigma_w^3}\dot{\gamma}\left(\sigma^3,\ T\right)d\sigma^3 \tag{5}$$

where T is temperature. From Eq. (5), V_S is obtained by plotting $\dot{\gamma}_A$ as a function of the inverse of diameter of die, $1/D$, i.e., the slope of the resultant graph corresponds to $8V_S$ (The Mooney method). Furthermore, the slip velocity V_S can be estimated without performing experiments with various diameters of dies using the modified Mooney method. In the modified Mooney method, the polymeric fluid is assumed to be a power law fluid ($\sigma = K(\dot{\gamma})^n$), and the slip velocity V_S is expressed by the following equation as

$$V_S = \frac{D}{8}\left[\dot{\gamma}_A - \frac{4n}{3n+1}\left(\frac{\sigma_w}{K}\right)^{\frac{1}{n}}\right] \tag{6}$$

where K is the power law coefficient and n is the flow index.

In order to estimate the extensional strain rates $\dot{\varepsilon}$, extensional stress τ, extensional viscosity η_E, and entry pressure loss ΔP_{ent} at the entrance to the capillary which are relevant to the melt-fracture, we used Cogswell's method [10–13,20,23]. Cogswell's method is the widely used method to estimate the elongational behavior at high extensional strain rates from capillary data.

$$\dot{\varepsilon} = \frac{4\sigma_W\dot{\gamma}_A}{3(n+1)\Delta P_{ent}} = \frac{\dot{\gamma}_A\tan\alpha}{2} \tag{7}$$

$$\tau = \frac{3(n+1)\Delta P_{ent}}{8} = \frac{\sigma_w}{\tan\alpha} \tag{8}$$

$$\eta_E = \frac{9(n+1)^2\Delta P_{ent}^2}{32\eta_s\dot{\gamma}_A^2} \tag{9}$$

where η_s is the shear viscosity.

3. Results and discussion

3.1. Rheological characterization

Fig. 2 depicts the master curves of the storage modulus G' and the magnitudes of complex viscosity $|\eta^*|$ of PS1-3 as a function of frequency ω where the reference temperature T_r is set to 210 °C and data at the five temperatures 180, 195, 210, 225 and 240 °C are superposed using the so-called shift factor a_T. The storage moduli G''s of PS1-3 are enhanced with the molecular weight at a low

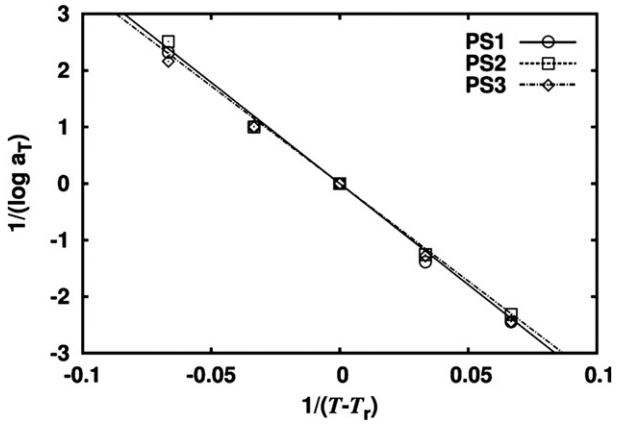

Fig. 3. WLF plot for the shift factors of PS1-3 using $T_r = 210$ °C.

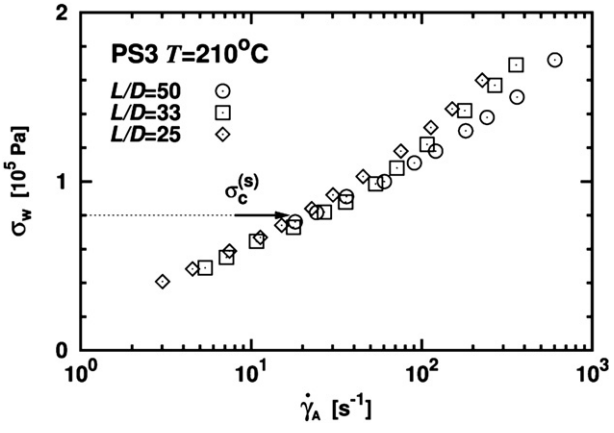

Fig. 4. Flow curves of PS3 at 210 °C observed by using capillaries with different $L/D = 25$, 33 and 50.

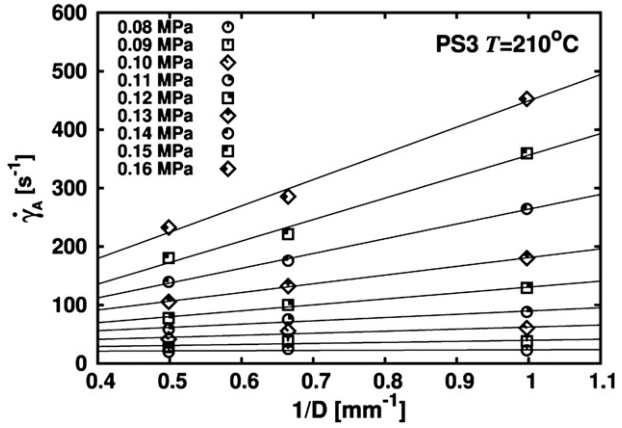

Fig. 5. Wall shear rate $\dot{\gamma}_A$ as a function of the inverse of diameter of die $1/D$ for various wall stresses. Their slopes of the lines corresponds to $8V_s$.

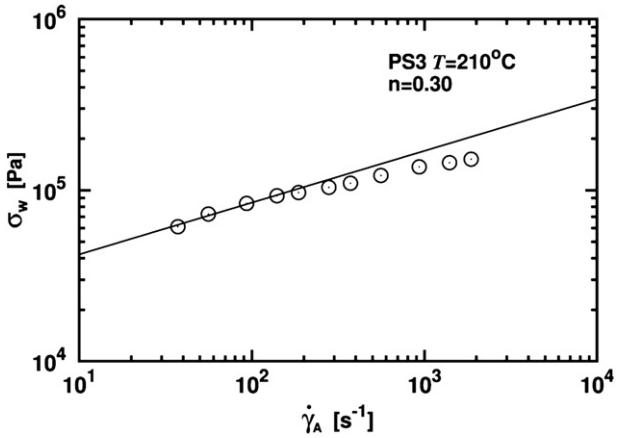

Fig. 7. Flow curve using obtained wall shear rate of PS3 at 210 °C using $L/D = 20$.

frequency region. At a high frequency region, G''s approach a plateau modulus (G_N^0) irrespective of the frequency and the molecular weight. From the comparison of $|\eta^*|$ among PS1-3, we can see that the zero-shear viscosity increases with the molecular weight and the shear thinning tends to start at a lower frequency region with the increase of molecular weight. In this study, we used the three types of samples with the similar molecular weight distribution *i.e.*, M_w/M_n's are almost the same (see Table 1). Therefore, it is considered that these behaviors of G′ and $|\eta^*|$ are originating from the difference in the relaxation time that is enhanced with increase of molecular weight. The WLF plot of $1/(\log a_T)$ versus $1/(T - T_r)$ is shown in Fig. 3. From the Fig. 3, it is found that the shift factor a_T is in good agreement with the WLF equation:

$$\ln a_T = -\frac{C_1(T - T_r)}{C_2 + T - T_r} \tag{10}$$

where C_1 and C_2 are constants. From the master curves of the G′ and $|\eta^*|$ at $T_r = 210$ °C, the shift factor a_T is found to be a constant and independent of frequency and molecular weight, and turns out to be 10.00 at 180 °C, 0.165 at 240 °C.

3.2. Capillary rheometer studies

In Fig. 4, we show the flow curves of PS3 at 210 °C for three cases of L/D. When we use dies with an entry angle ($2\alpha = 60°$, see Fig. 1 and Table 2) and with enough length L for the measurement of slip phenomena and unstable flow phenomena, we did not perform the Bagley correction, i.e., we neglected the pressure loss, on the other hand, when we use dies with the entry angle $2\alpha = 180°$, the Bagley correction is applied to the estimation of the wall shear stress σ_w. As seen from Fig. 4, we can see deviations of flow curves at above around $\sigma_w \cong 0.09$ MPa. Such a behavior could not be observed in PS1 and PS2. In the case of PS3, the appearance of deviations of flow curves at a stress more than a certain value implies that a slippage starts to occur from the corresponding shear rate. In order to evaluate the slip velocity V_s using Eq. (5), we plot the shear rate $\dot{\gamma}_A$ as a function of the inverse of diameter of die, $1/D$ in Fig. 5. The slope of the graph in Fig. 5 corresponds to $8V_s$. As seen from Fig. 5, the graph for $\sigma = 0.08$ MPa is almost flat, but the graphs for $\sigma \geq 0.09$ MPa have non-zero slopes. The obtained slip velocities are shown in Fig. 6. We also applied the modified Mooney method to the estimation of the slip velocity without performing experiments with various diameters of dies. Firstly we confirmed whether the slip velocity of the sample PS3 shows the simple power law

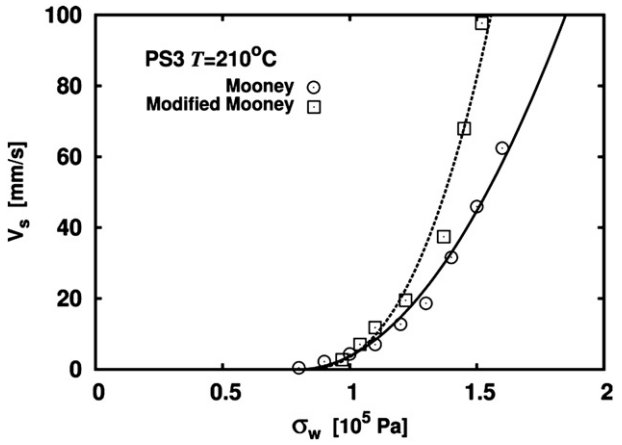

Fig. 6. Comparison of the slip velocities evaluated by the Mooney method and the modified Mooney method for PS3 at 210 °C. The slip velocities are fitted by using Eq. (11) and $\sigma_c^{(s)} = 0.08$ MPa estimated by the analyses in Figs. 4 and 5. By the fitting, $a = 58.3$ mm/s and $m = 1.99$ in the Mooney method, and $a = 115$ mm/s, $\sigma_c^{(s)} = 0.08$ MPa, and $m = 2.53$ in the modified Mooney method are obtained.

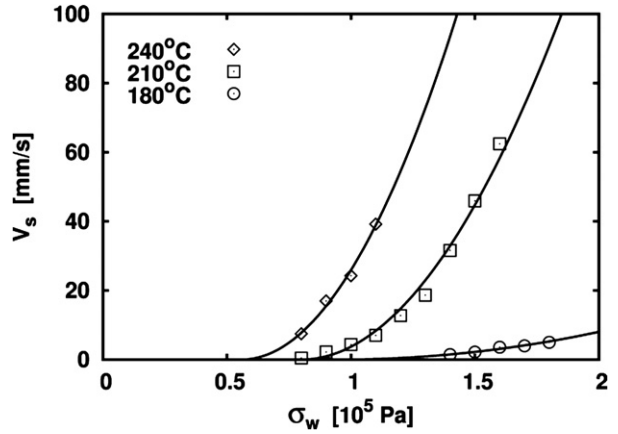

Fig. 8. Slip velocities of PS3 as a function of the wall shear stress σ_w at the temperatures 180, 210, 240 °C. The slip velocities are fitted by using Eq. (11) and $m = 1.99$obtained by the analysis in the Mooney method of Fig. 6. By the fitting, $a = 41.5$ mm/s and $\sigma_c^{(s)} = 0.056$ MPa at 240 °C, $a = 58.3$ mm/s and $\sigma_c^{(s)} = 0.08$ MPa at 210 °C and $a = 6.5$ mm/s and $\sigma_c^{(s)} = 0.095$ MPa at 180 °C are obtained.

Table 3
Temperature dependence of the slip coefficient a, the index m, and the critical slip stress $\sigma_c^{(s)}$ for PS3 and HDPE.

Resin	T [°C]	a [mm/s]	m	$\sigma_C^{(S)}/10^5$ [Pa]
PS3	180	6.5	1.99	0.95
	210	58.3	1.99	0.80
	240	41.5	1.99	0.56
HDPE	180	0.9	3.06	0.90
	200	1.2	2.95	–

behavior as a function of the wall stress σ_w or not. As mentioned above, since we used dies with an entry angle ($2\alpha = 180°$) and $L/D = 20$ for the measurement of modified Mooney method, we used the Bagley correction to estimate the shear stress σ_w. Then the flow curve is shown in Fig. 7. As seen from Fig. 7, the flow curve almost obeys a power law, but in the higher shear rate region the flow curve deviates from a guide line obtained by a fitting of data to a power law function in a lower shear rate region. By the fitting of the flow curve data less than $\dot{\gamma}_A = 180\ s^{-1}$ to the power law function, the flow index n and the power law factor K are found to be $n = 0.303$ and $K = 0.0210$ MPa $(s)^n$. Using the power law expression for this sample, now we can estimate the slip velocities by Eq. (6), and also plot them in Fig. 6. As seen from Fig. 6, the wall stress dependence of the slip velocity V_s can be expressed empirically by the following equation

$$V_s(\sigma_w) = \begin{cases} a\cdot\left(\frac{\sigma_w-\sigma_c^{(s)}}{\sigma_c^{(s)}}\right)^m & \text{for } \sigma_w \geq \sigma_w^{(s)} \\ 0 & \text{for } \sigma_w < \sigma_w^{(s)} \end{cases} \quad (11)$$

where a is the slip coefficient. In the fitting of slip data in the Mooney and modified Mooney method in Fig. 6 with Eq. (11), we set the critical slip stress to 0.08 MPa according to the result of Figs. 4 and 7. As seen from Fig. 6, it is found that the slip velocity estimated by the modified Mooney method is a little bit higher than that evaluated by the Mooney method. The similar behavior is observed by Hatzikiriakos et al. [9]. They also found that the slip velocity decreases with the increase of L/D ratio, and discussed that the origin of L/D ratio dependence of the slip velocity comes from the errors related to the pressure loss at the entrance of die since in the modified Mooney method the Bagley correction is not applied to the estimation of stress. In our experiments, since L/D of die used in the modified Mooney method ($L/D = 20$) is smaller than that in the Mooney method ($L/D = 25$,33,50), it is considered that the slip velocity estimated by the modified Mooney method became larger than that by the Mooney method in similar fashion to the result of Hatzikiriakos et al. As for the critical slip stress $\sigma_c^{(s)}$, the both methods resulted in almost the same value $\sigma_c^{(s)} \cong 0.08$ MPa as seen from the Figs. 4 and 7. From the fitting data in Fig. 8 (and those in Fig. 13 where the modified Mooney method is used), it seems that the exponent in eq. (11) is approximately $m \cong 2.0$ in the Mooney method and $m \cong 2.5$ in the modified Mooney method. Actually, if we take $m = 2.0$ and $m = 2.5$ in the fittings of the slip data obtained in the Mooney and modified Mooney method respectively, the fitted lines are almost the same with those in Figs. 8 and 13 on the exterior. We show the temperature dependence of the slip velocity for PS3 in Fig. 8. In Fig. 8, we also show the fitted lines to the data at $T = 180$ °C and 240 °C by Eq. (11) with $m = 1.99$ obtained by the fitting of data at $T = 210$ °C in the Mooney method. By the fittings, we estimated the slip coefficient a and the critical slip stress $\sigma_c^{(s)}$ at $T = 180$ °C and 240 °C. As seen from the Fig. 8, the data of slip velocity are nicely fitted by eq. (11) with the constant exponent $m = 1.99$, which supports the result reported by Hatzikiriakos et al. [9] where m is not a function of temperature, but the coefficient a is an increasing function of temperature. The temperature dependence of a, and critical slip stress $\sigma_c^{(s)}$ are shown

Table 4
Molecular weight and temperature dependence of the slip velocity of PS at $\sigma_w = 0.1$ MPa.

Slip Velocity V_S [mm/sec]			
	180 °C	210 °C	240 °C
PS1 ($M_w = 192{,}000$)	0	0	0
PS2 ($M_w = 258{,}000$)	0	0	0
PS3 ($M_w = 321{,}000$)	0.0298	3.96	39.6

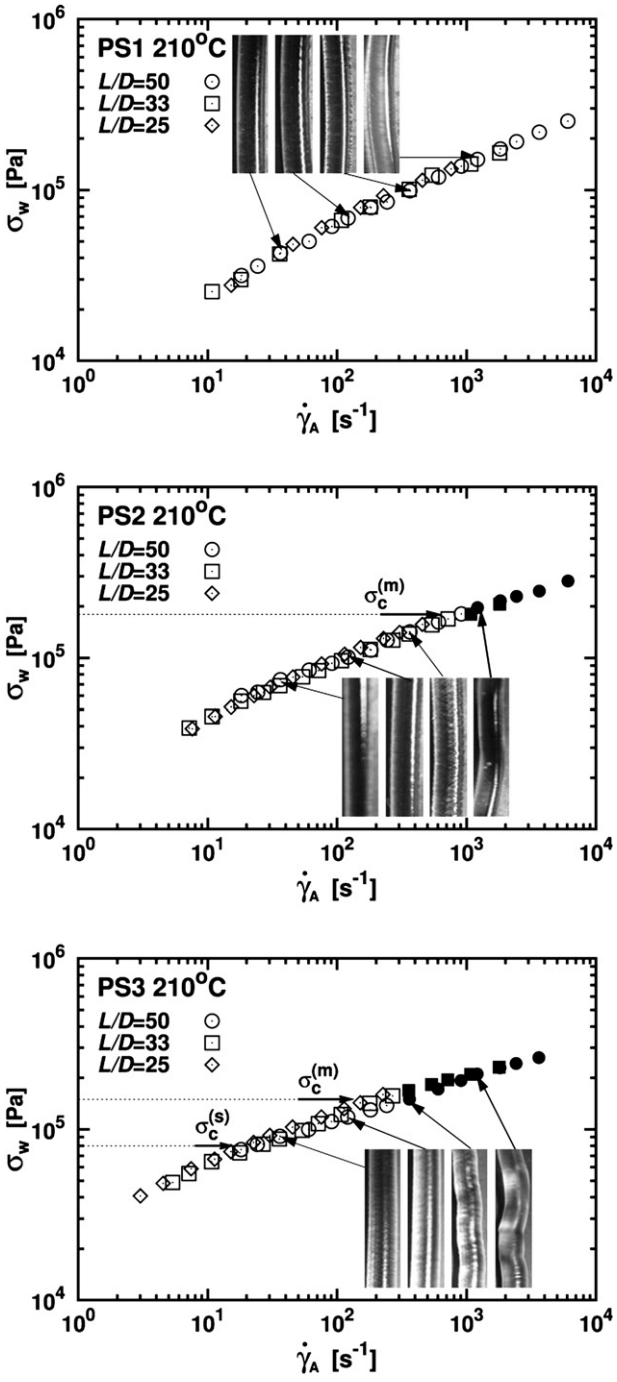

Fig. 9. Flow curves and morphology of extrudates for PS1-3 at 210 °C. The morphology of extrudates obtained in $L/D = 50$ at $\dot{\gamma}_A = 3.65 \times 10^1$, 1.22×10^2, 3.65×10^2, 1.22×10^3 s^{-1}.

Table 5
Temperature dependence of the critical melt-fracture shear rate $\dot{\gamma}_c^{(m)}$, critical melt-fracture shear stress $\sigma_c^{(m)}$, extensional strain rate $\dot{\varepsilon}_c^{(m)}$ and critical melt-fracture extensional stress $\tau_c^{(m)}$.

Polymer	180 °C				210 °C				240 °C			
	$\dot{\gamma}_c^{(m)}$ [S^{-1}]	$\sigma_c^{(m)}$ [MPa]	$\dot{\varepsilon}_c^{(m)}$ [S^{-1}]	$\tau_c^{(m)}$ [MPa]	$\dot{\gamma}_c^{(m)}$ [S^{-1}]	$\sigma_c^{(m)}$ [MPa]	$\dot{\varepsilon}_c^{(m)}$ [S^{-1}]	$\tau_c^{(m)}$ [MPa]	$\dot{\gamma}_c^{(m)}$ [S^{-1}]	$\sigma_c^{(m)}$ [MPa]	$\dot{\varepsilon}_c^{(m)}$ [S^{-1}]	$\tau_c^{(m)}$ [MPa]
PS1	456	0.26	132	0.45	–	–	–	–	–	–	–	–
PS2	108	0.20	31	0.35	760	0.17	219	0.30	–	–	–	–
PS3	27	0.16	8	0.28	362	0.15	105	0.26	1081	0.13	312	0.23

in Table 3. From the results, the slip velocity increases and the critical slip stress $\sigma_c^{(s)}$ decreases with the temperature (see Table 3). As a reference, the temperature dependence of the slip velocity in HDPE observed by Hatzikiriakos et al. [9,10] is also shown in Table 3. The coefficient a in PS depends on the temperature in similar fashion to the behavior of HDPE. The temperature dependence of a in PS3 is much larger than that in HDPE. This is simply because of the difference in the temperature dependence of shear stress, namely, the difference in the activation energy E_a between PS and HDPE. Actually, the activation energy E_a of PS is found to be 125 kJ/mol from our dynamic shear experiments, and E_a of HDPE is usually about 30 kJ/mol [24]. In order to examine the molecular weight dependence of slip phenomenon for PS, we tried to obtain the slip velocity for PS1 and PS2 using the Mooney method. However, we could not observe a slip phenomenon in PS1 and PS2 in the temperature range from 180 °C to 240 °C (see Table 4). The mechanism of the wall slip phenomenon has been studied from experimental approach and from theoretical and numerical approaches using a variety of viscoelastic models [2,9,10,14–16]. Wu et al. [17] have argued that the wall slip is an adhesive failure between the wall and the polymer chains, because they have considered that the wall slip occurs when the shear stress at the wall is greater than the adhesive stress between the wall and polymer chains. On the other hand, the wall slip can be considered to be the adsorption-desorption alternate process of polymer chains on the wall. In this case, the slip velocity is expected to be decreased with decrease of molecular weight. Blyler Jr. et al. [18] have reported that the slip velocity decreases with decrease of molecular weight in HDPE. Furthermore, Jabbarzadeh et al. [19] have also reported that the slip velocity decreases with decrease of molecular weight by molecular-dynamics simulations. As seen from Table 4, the slip velocity becomes zero by decreasing the molecular weight in PS. Our result supports their results. We are considering the reason why the PS1 and PS2 do not exhibit the slip behavior as follows. The slip phenomenon at the wall is greatly related to deformation and relaxation of polymer chains in the vicinity of the wall, and therefore will be highly sensitive to the molecular weight. Although the difference in molecular weights between PS2 and PS3 are not so large, the stress relaxation times of PS2 and PS3 are greatly different (see Table 1 and Fig. 2). We are considering that the shorter relaxation times in PS1 and PS2 makes the critical slip stresses in these systems higher ones which are much larger than our experimentally accessible stress or makes the slip velocities in these systems too small to estimate them by the Mooney methods.

At a shear rate region higher than the one where a slip takes place, on the other hand, we observed a melt-fracture. In Fig. 9, we show not only the flow curve of PS1-3 at 210 °C with capillaries of $D = 1, 1.5, 2$ mm and $L = 50$ mm but also the morphology of extrudates obtained at $L/D = 50$ at $\dot{\gamma}_A = 3.65 \times 10^1,\ 1.22 \times 10^2,\ 3.65 \times 10^2,\ 1.22 \times 10^3\ s^{-1}$. The distortion of extrudate starts to appear from a critical shear rate and shear stress. Hereafter we will refer them to the critical melt-fracture shear rate $\dot{\gamma}_c^{(m)}$ and shear stress $\sigma_c^{(m)}$, respectively. At a stress higher than $\sigma_c^{(m)}$, the pressure and the shear stress oscillate between two values owing to an unstable flow. This phenomenon is known as the oscillating melt-fracture [4–7]. In our experiments, we could not observe a clear transition from an unstable flow with a helical-shaped extrudate to melt-fracture, although such a transition has been observed in type II materials [25]. In Fig. 9, the filled symbol are used for data at a shear stress higher than the critical melt-fracture shear stress $\sigma_c^{(m)}$, because of the unstable pressure. This means that the critical stress and shear rate for the onset of melt-fracture are not sensitive to L/D, i.e., the oscillating melt-fracture originates from a flow instability in the barrel. Ballenger et al. [4,5] have reported that a spiraling flow at the entrance of capillary occurs above a certain critical shear rate, and then a distorted extrudate with a helical form appears. It is now generally accepted that the melt-fracture is initiated at the entrance to a capillary die where the melt undergoes primarily uniaxial extension due to the contraction flow. In Table 5, we show the critical melt-fracture shear rate $\dot{\gamma}_c^{(m)}$, shear stress $\sigma_c^{(m)}$, extensional strain rate $\dot{\varepsilon}_c^{(m)}$ and extensional stress $\tau_c^{(m)}$ of PS1-3 at 180, 210 and 240 °C. The critical melt-fracture shear rate $\dot{\gamma}_c^{(m)}$ increases with temperature and molecular weight. The critical melt-fracture shear stress $\sigma_c^{(m)}$ and extensional stress $\tau_c^{(m)}$ decrease with increase of molecular weight. Everage Jr. et al. [8] have reported that $\dot{\gamma}_c^{(m)}$ depends on the entrance angle, but the critical melt-fracture extensional strain rate $\dot{\varepsilon}_c^{(m)}$ estimated by using their observed flow behavior around the entrance is independent of the entrance angle. Namely, the onset of melt-fracture should be discussed through the physical properties for extensional flow. Since it is considered that the melt-fracture is greatly affected by the extensional flow at the capillary inlet [4–8,21,22], we investigated the effect of extensional stress τ on the onset of melt-fracture. From analyses for PS1-3 at 180, 210 and 240 °C using Cogswell's method, we obtained the critical melt-fracture extensional stresses $\tau_c^{(m)}$ as functions of the critical melt-

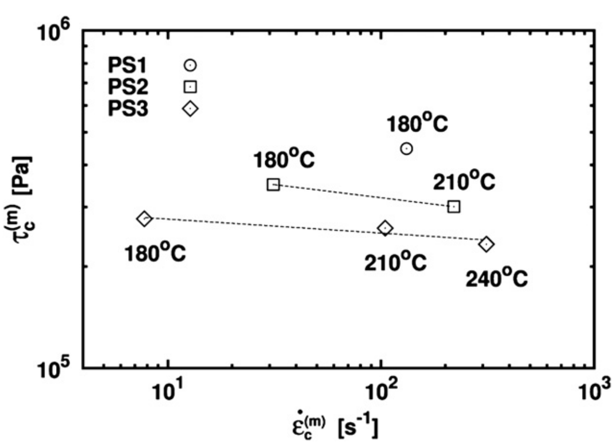

Fig. 10. Critical melt-fracture extensional stresses $\tau_c^{(m)}$ of PS1-3 at 180–240 °C as a function of critical melt-fracture extensional strain rate $\dot{\varepsilon}_c^{(m)}$. The dotted line are obtained by fitting the data with the equation $\tau_c^{(m)} = A(\dot{\varepsilon}_c^{(m)})^{-\alpha}$ in which $\alpha = 7.7 \times 10^{-2}$ and $A = 0.45$ MPa (s)$^{\alpha}$ in PS2 and $\alpha = 4.1 \times 10^{-2}$ and $A = 0.30$ MPa (s)$^{\alpha}$ in PS3.

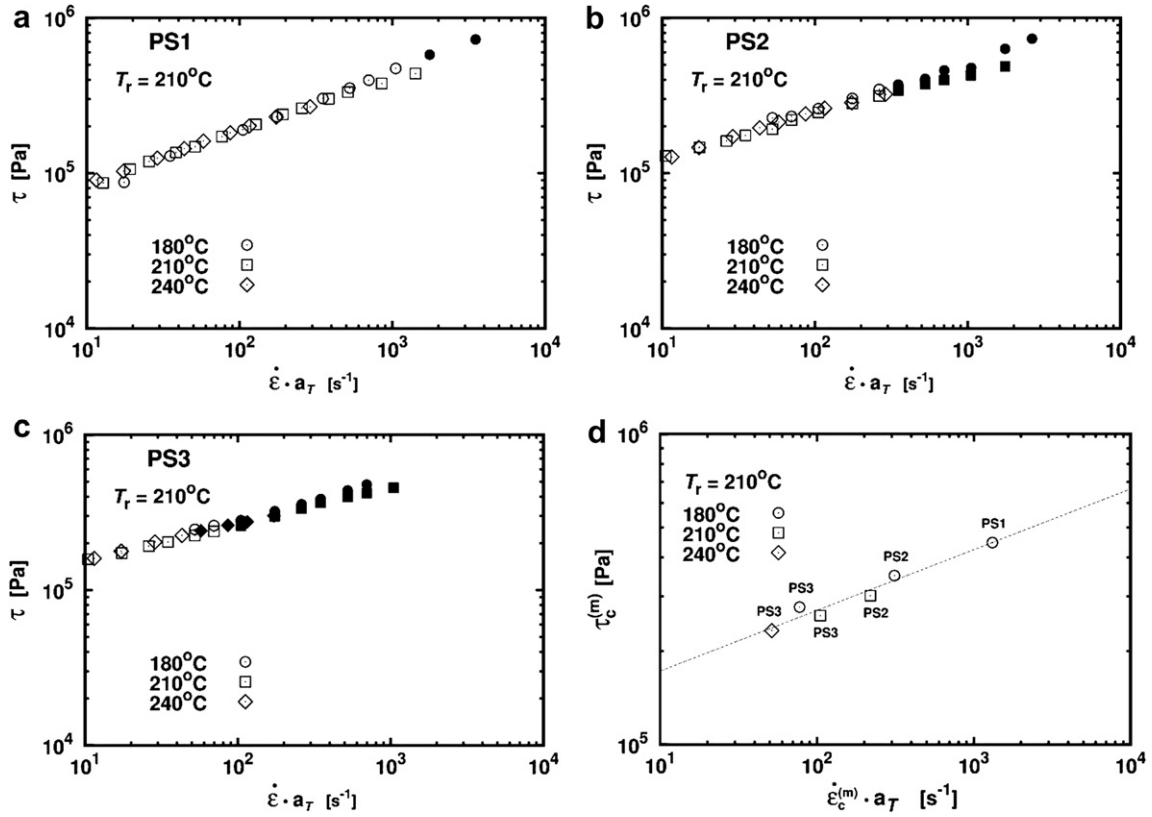

Fig. 11. Master curves of extensional stresses as a function of extensional strain rate for (a) PS1, (b) PS2 and (c) PS3 at $L/D = 50$. (d) Master curve of critical melt-fracture extensional stress $\tau_c^{(m)}$ as a function of $\dot{\varepsilon}_c^{(m)} \cdot a_T$. The dotted line in (d) is obtained by fitting the data with a function $\tau_c^{(m)} = \alpha \cdot (\dot{\varepsilon}_c^{(m)})^{\beta}$ and the parameters are found to be $\alpha = 0.11$ MPa·(s)$^{-\beta}$, $\beta = 0.20$. The reference temperatures T_r to the master curves in (a)–(d) are set to 210 °C and the shift factors a_T's for PS1-3 obtained in Fig. 2 are used.

fracture extensional strain rate $\dot{\varepsilon}_c^{(m)}$ as shown in Fig. 10. We could not observe the critical melt-fracture extensional strain rate $\dot{\varepsilon}_c^{(m)}$ in PS1 at 180 °C and 210 °C, and in PS2 at 180 °C. As seen from Fig. 10, the critical melt-fracture extensional stress $\tau_c^{(m)}$ for each samples slightly decreases with temperature, although it has already reported by Combeaud et al. [25] that $\tau_c^{(m)}$ does not depend on temperature. On the other hand, the critical melt-fracture extensional strain rate $\dot{\varepsilon}_c^{(m)}$ significantly decreases with temperature, which means the extensional stress is essential to whether a melt-fracture takes place or not. The critical melt-fracture extensional stress $\tau_c^{(m)}$ decreases with the increase of the molecular weight. In other words, the melt-fracture easily occurs with increase of molecular weight, while the extensional stress for the onset of melt-fracture is not sensitive to temperature. The reason why we could not observe the critical melt-fracture extensional stress $\tau_c^{(m)}$ in PS1 at 210 °C and 240 °C, and in PS2 at 240 °C is that the extensional stress did not reach the critical melt-fracture extensional stress $\tau_c^{(m)}$ within the experimentally accessible extensional strain rate ($\dot{\varepsilon} \leq 10^3$ s^{-1}). In Fig. 11(a)–(c), we show the master curve of extensional stress τ of PS1-3 at $L/D = 50$ as a function of extensional strain rate $\dot{\varepsilon}$ where the reference temperature is 210 °C and the shift factor a_T is estimated in Fig. 2. As seen from Fig. 11(a)–(c), the flow curves can be overlapped by using the shift factor a_T's at extensional strain rates lower than $\dot{\varepsilon}_c^{(m)}$ (in other words, at the extensional stress lower than a critical melt-fracture extensional stress $\tau_c^{(m)}$). Since the critical melt-fracture point ($\dot{\varepsilon}_c^{(m)}$, $\tau_c^{(m)}$) is the end of the master curve, we can expect that the critical melt-fracture extensional stress $\tau_c^{(m)}$ as a function of $\dot{\varepsilon}_c^{(m)}$ follows the time–temperature superposition principle, i.e., the temperature dependence of the critical melt-fracture extensional stress $\tau_c^{(m)}$ and strain rate $\dot{\varepsilon}_c^{(m)}$ comes from that of viscoelastic behavior of PS. In order to confirm this point, in Fig. 11(d) we plotted $\tau_c^{(m)}$'s as a function of $\dot{\varepsilon}_c^{(m)} \cdot a_T$ where a_T is the shift factor estimated in Fig. 2 and one can clearly see the time–temperature superposition also holds for the $\tau_c^{(m)}$ versus $\dot{\varepsilon}_c^{(m)}$ curve. In Fig. 12, we show the temperature dependence of the critical melt-fracture extensional stress $\tau_c^{(m)}$ and the critical slip stress $\sigma_c^{(s)}$. As seen from Fig. 12, the critical slip stress $\sigma_c^{(s)}$ decreases with the temperature, on the other hand, the critical melt-fracture extensional stress $\tau_c^{(m)}$ *weakly* decreases

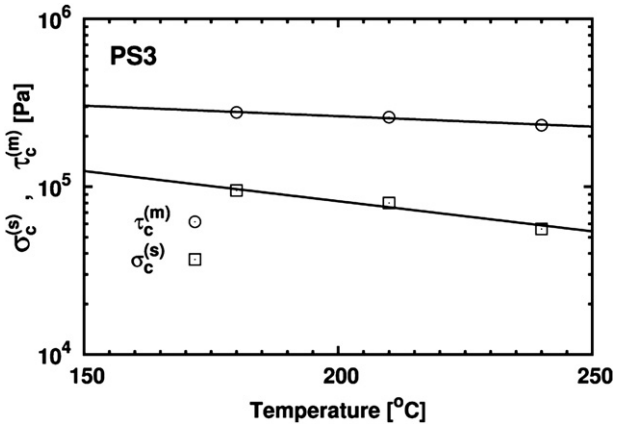

Fig. 12. Temperature dependence of the critical slip shear stress $\sigma_c^{(s)}$ and the critical melt-fracture extensional stress $\tau_c^{(m)}$. The solid lines are obtained by fitting the data with the equation $\sigma_c^{(s)}(\tau_c^{(m)}) = B\exp(-T/T_o)$ in which $B = 4.11$ MPa, $T_o = 121$ K for slip and $B = 1.03$ MPa, $T_o = 348$ K for melt-fracture.

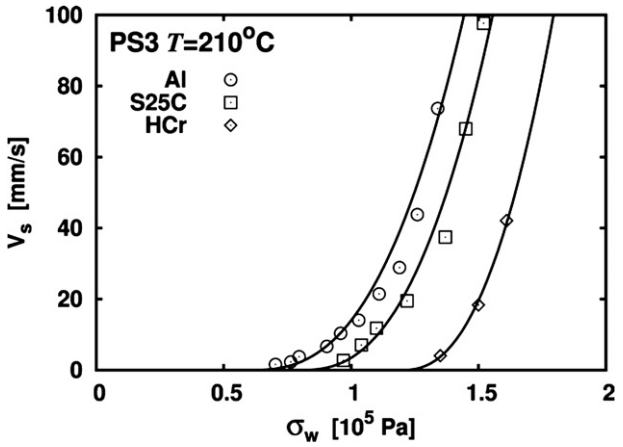

Fig. 13. Slip velocities of PS3 in dies made of three kinds of materials (S25C, Al and HCr) at 210 °C. Slip velocities are estimated by the modified Mooney method and are fitted by using Eq. (11). By the fitting, $a = 40.7$ mm/s, $\sigma_c^{(s)} = 0.06$ MPa and $m = 2.64$ in Aluminum die, $a = 115$ mm/s, $\sigma_c^{(s)} = 0.08$ MPa, and $m = 2.53$ in S25C die, and $a = 533.8$ mm/s, $\sigma_c^{(s)} = 0.12$ MPa, and $m = 2.38$ in HCr die are obtained.

with the temperature as compared with $\sigma_c^{(s)}$. Namely, the onset of melt-fracture is affected mainly by the extensional stress, and the wall slip seems to be related with a temperature sensitive physical property and tends to easily occur with increase of temperature.

In order to investigate the dependence of the slip velocity on the wall material of die, we used the dies made of (a) S25C, (b) Aluminum and (c) HCr (see Table 2 for details). The S25C is composed of the carbon (0.22–0.28%), silicon (0.15–0.35%), manganese (0.30–0.60%), phosphorus (<0.030%), and sulfur (<0.035%) (*cf.* JIS G 4051). Firstly we tried to make a HCr-plated die with the entry angle ($2\alpha = 60°$), however, we could not have such a die since there were some difficulties in plating the inside of a capillary die having the entry angle $2\alpha = 60°$with Chrome, which forced us to use dies with the entry angle ($2\alpha = 180°$) in our investigation of the effect of wall material of die on slippage. Since we used dies with the entry angle ($2\alpha = 180°$) for investigations of the effect of wall material of die on the flow behavior, we estimated the corrected wall stress σ_w from the Bagley correction. The slip velocities in the three types of die (a)–(c) are estimated by the modified Mooney method. In Fig. 13 we show the obtained slip velocities for PS3 at 210 °C by using these three types of dies and fitted lines by using eq. (11). The procedure of fitting of data using eq. (11) is almost the same with the one used in Fig. 6 for S25C. In the fitting of data in Al and HCr, firstly we determined the critical slip stresses to be 0.06 MPa and 0.12 MPa, respectively. Then we fit the data with the Eq. (11) through two parameters a and m. We found that the critical slip stress $\sigma_c^{(s)}$ *does* depend on the wall material of die, and $\sigma_c^{(s)}$ of the Aluminum die is the smallest and $\sigma_c^{(s)}$ of HCr is the largest in these three dies, i.e., $\sigma_c^{(s)}(\mathrm{Al}) < \sigma_c^{(s)}(\mathrm{S25C}) < \sigma_c^{(s)}(\mathrm{HCr})$. In order to understand the reason why the slippage is more easily happened in the die made of Aluminum than the other two dies, the more detail investigation for the surface properties of die against polystyrene will be needed.

4. Conclusion

We investigated the slip phenomena and unstable flow phenomena in PS melts as one of Type II samples using a capillary rheometer. Furthermore, the effect of wall material on the slip phenomena of the PS melts was also investigated. Our finding can be summarized as follows,

I. The slip velocities estimated by the modified Mooney method is nicely fitted by the Eq. (11). The slip velocity obtained in the modified Mooney method is a little bit higher than that evaluated by the Mooney method in accordance with the result of Hatzikiriakos et al. [9]. On the other hand, as for the critical slip stress $\sigma_c^{(s)}$, the two methods result in almost the same value, $\sigma_c^{(s)} = 0.08$ MPa at $T = 210$ °C. It seems that the slip exponent m in eq. (11) is approximately $m \cong 2.0$ in the Mooney method and $m \cong 2.5$ in the modified Mooney method. Furthermore, the slip velocity increases and the critical slip stress $\sigma_c^{(s)}$ decreases with the temperature. We also found that the wall slip tends to easily occur with increase of the temperature and molecular weight.

II. At a shear rate region higher than the one where a slip takes place, we observed a melt-fracture. The critical melt-fracture extensional stress $\tau_c^{(m)}$ slightly decreases with temperature and $\tau_c^{(m)}$ decreases with increase of the molecular weight. In other words, the melt-fracture easily occurs with increase of molecular weight, while the extensional stress for the onset of melt-fracture is not so sensitive to temperature. Since the flow curves can be overlapped by using the shift factor a_T's estimated in Fig. 2 at extensional strain rates lower than $\dot{\varepsilon}_c^{(m)}$, it is found that the critical melt-fracture extensional stress $\tau_c^{(m)}$ as a function of $\dot{\varepsilon}_c^{(m)}$ follows the time–temperature superposition principle, i.e., the temperature dependence of the function $\tau_c^{(m)}$ of $\dot{\varepsilon}_c^{(m)}$ comes from that of viscoelastic behavior of PS.

III. In order to investigate the dependence of the slip velocity on the wall material of die, we used the dies made of (a) S25C, (b) Aluminum and (c) HCr. We found that the critical slip stress $\sigma_c^{(s)}$ does depend on the wall material of die, and $\sigma_c^{(s)}$ of the Aluminum die is the smallest and $\sigma_c^{(s)}$ of HCr is the largest, i.e., $\sigma_c^{(s)}(\mathrm{Al}) < \sigma_c^{(s)}(\mathrm{S25C}) < \sigma_c^{(s)}(\mathrm{HCr})$.

Acknowledgement

This work was supported by KAKENHI (Grant-in-Aid for Scientific Research) on Priority Area "Soft Matter Physics" from the Ministry of Education, Culture, Sports, Science and Technology of Japan.

References

[1] Mooney M. J Rheo 1931;2:210.
[2] Kalika DS, Denn MM. J Rheo 1987;31:815.
[3] Ramamurthy AV. J Rheo 1986;30:337.
[4] Ballenger TF, White JL. J Appl Polym Sci 1971;15:1949.
[5] Ballenger TF, Chen IJ, Crowder JW, Hagler GE, Bogue DC, White JL. Trans Soc Rheol 1971;15:195.
[6] Kim S, Dealy JM. Polym Eng Sci 2002;42:482.
[7] Kometani H, Kitajima H, Matsumura T, Suga T, Kanai T. Seikei-Kakou 2007;19:118.
[8] Everage Jr AE, Ballman RL. J Appl Polym Sci 1974;18:933.
[9] Hatzikiriakos SG, Dealy JM. J Rheo 1992;36:703.
[10] Hatzikiriakos SG, Dealy JM. J Rheo 1991;35:497.
[11] Cogswell FN. Polym Eng Sci 1972;12:64.
[12] Cogswell FN. Trans Soc Rheol 1972;16:383.
[13] Cogswell FN. J Non-Newtonian Fluid Mech 1978;4:23.
[14] Ho TC, Denn MM. J Non-Newtonian Fluid Mech 1977;3:179.
[15] Lee KC, Finlayson BA. J Non-Newtonian Fluid Mech 1986;21:65.
[16] Renardy M, Renardy Y. J Non-Newtonian Fluid Mech 1986;22:23.
[17] Wu S. Polym Int Afhe Dekker; 1982.
[18] Blyler Jr LL, Hart Jr AC. Polym Eng Sci 1970;10:193.
[19] Jabbarzadeh A, Atkinson JD, Tanner RI. Phys Rev E 2000;61(1):690.
[20] Rajagopalan D. Rheol Acta 2000;39:138.
[21] Denn MM, Marrucci G. AICHE J 1971;17:101.
[22] Hurlimann HP, Knappe W. Rheol Acta 1972;11:292.
[23] Kwag C, Vlachopoulos J. Polym Eng Sci 1991;31:1015.
[24] Laun HM. Prg Coll Polym Sci 1987;75:111.
[25] Combeaud C, Demay Y, Vergnes B. J Non-Newtonian Fluid Mech 2004;121:175.